To date, the beneficial effects of inhibiting TLR4 signaling have been shown in some experimental acute injury models using TLR4 mutant mice [6] and a lipid A analogue [10]. Since previous investigations have revealed no effect of TAK-242 on the function of the extracellular components (MD2 and CD14) and intracellular adaptor proteins (MyD88, TIRAP, TRIF and TRAM), the inhibitory effects of TAK-242 are considered to be due to the inhibition of signaling mediated by the intracellular domain of TLR4, such as the TIR domain [11, 25]. Mutational analysis using TLR4 mutants indicated that TAK-242 inhibits TLR4 signaling by binding to Cys747 in the intracellular domain of TLR4 [26]. Because of the small molecular size of 362 Da, TAK-242 can penetrate into tissues and cells and act directly on intracellular signaling pathways. TAK-242 inhibited MyD88-independent pathways as well as MyD88-dependent pathways and its inhibitory effect was largely unaffected by LPS concentration and types of TLR4 ligands [26]. TAK-242 had no effect on the LPS-induced conformational change of TLR4-MD-2 and TLR4 homodimerization. Therefore, TAK-242 might be effective in a variety of clinical settings.

The inflammatory cascade in ALI/ARDS is initiated by several inflammatory mediators, including pro-inflammatory cytokines and chemokines [27]. For example, TNF-α and IL-1 are early response cytokines that are produced in response to inflammatory stimuli, such as LPS or other microbial products [28]. In this study, TAK-242 strongly inhibited the production of these cytokines that promote the production of other mediators by macrophage, endothelial cells, fibroblasts, and epithelial cells.

In this study, we administered TAK-242 15 min before the intratracheal instillation. We previously showed that TAK-242 inhibited LPS lethality when administered 1 h before or simultaneous with intravenous LPS [12]. In this study, we examined whether TAK-242 is similarly effective on intratracheal stimuli. The time point of treatment was chosen because TAK-242 is supposed to be distributed in the whole body within 15 min.

Neutrophils have been recognized as important contributors to the pathogenesis of ALI/ARDS [29–31]. In addition, LPS is known to induce a large influx of neutrophils into the alveolar space [32]. In rodents, the two most important chemokines for neutrophil recruitment into the lung are KC and MIP-2 [15]. Since the production of these chemokines was significantly inhibited in the groups treated with TAK-242, we speculated that TAK-242 might attenuate neutrophil accumulation mainly via this inhibitory effect. In addition, TAK-242 treatment reduced the level of MPO, a parameter of neutrophil activation, in BAL fluid. It was indicated that TAK-242 might inhibit not only neutrophil accumulation, but also activation or degranulation in the alveolar space.

Since TAK-242 reduced the level of MPO in BAL fluid, treatment with TAK-242 has been suggested to inhibit not only neutrophil infiltration, but also activation or degranulation in the alveolar space. However, whether the effect of TAK-242 on neutrophil activation occurs through a direct effect on neutrophils or via an inhibitory effect on pro-inflammatory cytokines and chemokines remains to be determined.

Another limitation of our study was that we used LPS, not live bacteria, as an insult to induce lung injury. The TLR4 signaling pathway is important for host defense, especially against Gram-negative bacteria, as shown by the impaired defense of TLR4 mutant mice with pneumonia arising from infection with *Klebsiella pneumoniae* [33] and *Bordetella bronchiseptica* [34]. However, not all studies have shown that TLR4 is essential for adequate pulmonary host defense. For example, TLR4 mutant mice showed no difference in bacterial clearance following intranasal inoculation with *Legionella pneumophilia*, compared with a related substrain wild type for TLR4 [35]. TLR4 mutant mice also showed reduced inflammatory responses with no impairment in their ability to eliminate *E. coli* from the lungs [36]. Therefore, TLR4 may not be necessary for lung host defense against all Gram-negative bacteria, and we think that the inhibitory effects of TAK-242 on TLR4 signaling observed in the present study were not overestimated by our use of a lung injury model induced by LPS, and not live bacteria. In addition, we did not examine the effect of TAK-242 at later time points, because we focused on its effect on acute phase of lung injury. A preliminary experiment showed, however, a significant difference in the cell count in BAL fluid that was collected 12 h after LPS challenge [mean $\pm$ 1 SEM for the mice without TAK-242 treatment: 22.0 $\pm$ 1.1 ($\times 10^4$ per mL), whereas for those treated with 3.0 mg/kg of TAK-242: 8.5 $\pm$ 3.2 ($\times 10^4$ per mL); $P < 0.01$]. It was suggested that TAK-242 treatment might exert a beneficial effect on LPS-induced lung injury at later time points, which will be a subject of future investigation.

In conclusion, TAK-242 suppressed the LPS-induced production of inflammatory mediators, neutrophil recruitment in the lung, and the development of lung injury in a murine lung injury model. Neutrophils are responsible for both host defense against bacterial pathogens and tissue injury by releasing elastase and reactive oxygen species. In the clinical practice, most of the patients with ALI are treated with antibiotics. We think that, at least when bacterial activity is controlled by antibiotic therapy, blockade of the TLR4 signaling pathway might attenuate neutrophil-mediated lung injury rather than worsen bacterial infection.

Acknowledgments We thank Miyuki Yamamoto of Keio University School of Medicine and Masumi Uekata of Takeda

Pharmaceutical Co. Ltd. for their technical assistance. This study was supported in part by a grant-in-aid for scientific research from the Ministry of Health, Labour and Welfare of Japan (no. 19590913) (S. T.).

References

1. McIntyre RC Jr, Pulido EJ, Bensard DD, Shames BD, Abraham E. Thirty years of clinical trials in acute respiratory distress syndrome. Crit Care Med. 2000;28:3314–31.
2. Bersten AD, Edibam C, Hunt T, Moran J. Incidence and mortality of acute lung injury and the acute respiratory distress syndrome in three Australian states. Am J Respir Crit Care Med. 2002;165:443–8.
3. Brigham KL, Meyrick B. Endotoxin and lung injury. Am Rev Respir Dis. 1986;133:913–27.
4. Takeda K, Akira S. TLR signaling pathways. Semin Immunol. 2004;16:3–9.
5. Morrison DC, Ryan JL. Bacterial endotoxins and host immune responses. Adv Immunol. 1979;28:293–450.
6. Jeyaseelan S, Chu HW, Young SK, Freeman MW, Worthen GS. Distinct roles of pattern recognition receptors CD14 and Toll-like receptor 4 in acute lung injury. Infect Immun. 2005;73:1754–63.
7. Togbe D, Schnyder-Candrian S, Schnyder B, Couillin I, Maillet I, Bihl F, et al. TLR4 gene dosage contributes to endotoxin-induced acute respiratory inflammation. J Leukoc Biol. 2006;80:451–7.
8. Abraham E, Laterre PF, Garbino J, Pingleton S, Butler T, Dugernier T, et al. Lenercept (p55 tumor necrosis factor receptor fusion protein) in severe sepsis and early Lenercept (p55 tumor necrosis factor receptor fusion protein) in severe sepsis and early septic shock: a randomized, double-blind, placebo-controlled, multicenter phase iii trial with 1,342 patients. Crit Care Med. 2001;29:503–10.
9. Opal SM, Fisher CJ Jr, Dhainaut JF, Vincent JL, Brase R, Lowry SF, et al. Confirmatory interleukin-1 receptor antagonist trial in severe sepsis: a phase III, randomized, double-blind, placebo-controlled, multicenter trial. The interleukin-1 receptor antagonist sepsis investigator group. Crit Care Med. 1997;25:1115–24.
10. Shiozaki M, Doi H, Tanaka D, Shimozato T, Kurakata S. Syntheses of glucose analogues of E5564 as a highly potent anti-sepsis drug candidate. Bioorg Med Chem. 2006;14:3011–6.
11. Ii M, Matsunaga N, Hazeki K, Nakamura K, Takashima K, Seya T, et al. A novel cyclohexene derivative, ethyl (6*R*)-6-[*N*-(2-chloro-4-fluorophenyl)sulfamoyl]cyclohex-1-ene-1-carboxylate (TAK-242), selectively inhibits Toll-like receptor 4-mediated cytokine production through suppression of intracellular signaling. Mol Pharmacol. 2006;69:1288–95.
12. Sha T, Sunamoto M, Kitazaki T, Sato J, Ii M, Iizawa Y. Therapeutic effects of TAK-242, a novel selective Toll-like receptor 4 signal transduction inhibitor, in mouse endotoxin shock model. Eur J Pharmacol. 2007;571:231–9.
13. Shirley E. A non-parametric equivalent of Williams' test for contrasting increasing dose levels of a treatment. Biometrics. 1977;33:386–9.
14. Williams DA. A note on Shirley's nonparametric test for comparing several dose levels with a zero-dose control. Biometrics. 1986;42:183–6.
15. Olson TS, Ley K. Chemokines and chemokine receptors in leukocyte trafficking. Am J Physiol Regul Integr Comp Physiol. 2002;283:R7–28.
16. Hayden MS, West AP, Ghosh S. NF-κB and the immune response. Oncogene. 2006;25:6758–80.
17. Chow JC, Young DW, Golenbock DT, Christ WJ, Gusovsky F. Toll-like receptor-4 mediates lipopolysaccharide-induced signal transduction. J Biol Chem. 1999;274:10689–92.
18. Ulevitch RJ, Tobias PS. Receptor-dependent mechanisms of cell stimulation by bacterial endotoxin. Annu Rev Immunol. 1995;13:437–57.
19. Shimazu R, Akashi S, Ogata H, Nagai Y, Fukudome K, Miyake K, et al. MD-2, a molecule that confers lipopolysaccharide responsiveness on Toll-like receptor 4. J Exp Med. 1999;189:1777–82.
20. Wright SD, Ramos RA, Tobias PS, Ulevitch RJ, Mathison JC. CD14, a receptor for complexes of lipopolysaccharide (LPS) and LPS binding protein. Science. 1990;249:1431–3.
21. Christman JW, Lancaster LH, Blackwell TS. Nuclear factor kappa B: a pivotal role in the systemic inflammatory response syndrome and new target for therapy. Intensive Care Med. 1998;24:1131–8.
22. Xu WY, Wang L, Wang HM, Wang YQ, Liang YF, Zhao TT, et al. TLR2 and TLR4 agonists synergistically up-regulate SR-A in RAW264.7 through p38. Mol Immunol. 2007;44:2315–23.
23. Hirschfeld M, Ma Y, Weis JH, Vogel SN, Weis JJ. Cutting edge: repurification of lipopolysaccharide eliminates signaling through both human and murine toll-like receptor 2. J Immunol. 2000;165:618–22.
24. Xue Y, Yun D, Esmon A, Zou P, Zuo S, Yu Y, et al. Proteomic dissection of agonist-specific TLR-mediated inflammatory responses on macrophages at subcellular resolution. J Proteome Res. 2008;7:3180–93.
25. Kawamoto T, Ii M, Kitazaki T, Iizawa Y, Kimura H. Tak-242 selectively suppresses toll-like receptor 4-signaling mediated by the intracellular domain. Eur J Pharmacol. 2008;584:40–8.
26. Takashima K, Matsunaga N, Yoshimatsu M, Hazeki K, Kaisho T, Uekata M, et al. Analysis of binding site for the novel small-molecule TLR4 signal transduction inhibitor TAK-242 and its therapeutic effect on mouse sepsis model. Br J Pharmacol. 2009;157(7):1250–62.
27. Bhatia M, Moochhala S. Role of inflammatory mediators in the pathophysiology of acute respiratory distress syndrome. J Pathol. 2004;202:145–56.
28. Nathan CF. Secretory products of macrophages. J Clin Invest. 1987;79:319–26.
29. Steinberg KP, Milberg JA, Martin TR, Maunder RJ, Cockrill BA, Hudson LD. Evolution of bronchoalveolar cell populations in the adult respiratory distress syndrome. Am J Respir Crit Care Med. 1994;150:113–22.
30. Parsons PE, Fowler AA, Hyers TM, Henson PM. Chemotactic activity in bronchoalveolar lavage fluid from patients with adult respiratory distress syndrome. Am Rev Respir Dis. 1985;132:490–3.
31. Matthay MA. Conference summary: acute lung injury. Chest. 1999;116:119S–26S.
32. Reutershan J, Ley K. Bench-to-bedside review: acute respiratory distress syndrome—how neutrophils migrate into the lung. Crit Care. 2004;8:453–61.
33. Schurr JR, Young E, Byrne P, Steele C, Shellito JE, Kolls JK. Central role of Toll-like receptor 4 signaling and host defense in experimental pneumonia caused by gram-negative bacteria. Infect Immun. 2005;73:532–45.
34. Mann PB, Kennett MJ, Harvill ET. Toll-like receptor 4 is critical to innate host defense in a murine model of bordetellosis. J Infect Dis. 2004;189:833–6.
35. Lettinga KD, Florquin S, Speelman P, van Ketel R, van der Poll T, Verbon A. Toll-like receptor 4 is not involved in host defense against pulmonary *Legionella pneumophila* infection in a mouse model. J Infect Dis. 2002;186:570–3.
36. Lee JS, Frevert CW, Matute-Bello G, Wurfel MM, Wong VA, Lin SM, et al. TLR-4 pathway mediates the inflammatory response but not bacterial elimination in *E. coli* pneumonia. Am J Physiol Lung Cell Mol Physiol. 2005;289:L731–8.

講　座

ベクロニウムとスキサメトニウムは捨てがたい

武田純三*

[要旨] 本邦ではロクロニウムが諸外国から約10年遅れて2007年に発売され，発売後急速に使用量が増加している．しかし，世界ではベクロニウムもスキサメトニウムもまだ多くの国で使用されており，それなりの理由があると考えられる．ロクロニウムは速い作用発現，蓄積作用がなく持続投与が可能，水溶性であるなどの特徴があるが，作用持続時間はベクロニウムと変わりはなく，アナフィラキシー反応の発生頻度，集中治療患者への長期投与での蓄積の可能性，小児での使用に対する懸念が残されている．また，迅速導入時や帝王切開術の麻酔での筋弛緩薬として，さらに緊急事態発生時の使用には，スキサメトニウムが優れていると考えられ，ベクロニウムとスキサメトニウムはまだまだ捨てがたい筋弛緩薬といえる．

キーワード：ロクロニウム，ベクロニウム，スキサメトニウム，アナフィラキシー反応，迅速導入

(日臨麻会誌Vol.30 No.3, 438 ～ 445, 2010)

はじめに

ロクロニウムが日本で発売されてから，急速にその使用量が増えてきている．それに伴って，今まで使われてきたベクロニウムやスキサメトニウムの使用が激減してきている．しかし，これらの筋弛緩薬にはそれぞれ大きな特徴があり，その役目が終わったわけではなく，まだまだ捨てがたいものがある．

I　ロクロニウムとベクロニウム

日本で使用できる非脱分極性筋弛緩薬は，アミノステロイド系のみである(**図1**)．1973年に発売されたパンクロニウム，1988年に発売されたベクロニウムに次いで，世界に遅れること約10年後の2007年10月2日にロクロニウムが発売された．ロクロニウムをベクロニウムと比較すると，ロクロニウムではA-ringの3位にOHが結合することで水溶性として安定していることと，メチル基がアリル基に変わり効力が落ちていることがベクロニウムと異なっている．筋弛緩薬の作用発現時間は，力価に反比例することが知られており，力価の小さいロクロニウムは作用発現が速い．また，蓄積作用がなく，持続投与が可能なことも特徴としてあげられる．

ロクロニウムの発売以降，ロクロニウムのシェアが急速に増してきており，反対にベクロニウムの割合が低下してきている．2008年5月には逆転し，今後もロクロニウムがわが国では伸びていくものと思われる．しかし，海外ではロクロニウムは1990年代初めに発売され，使用されて以来10年以上を経過しているが，ロクロニウムがベクロニウムを駆逐するには至っておらず，現在もベクロニウムが臨床で使用されている(**図2**)．

*慶應義塾大学医学部麻酔学教室

著者連絡先　武田純三
〒160-8582　東京都新宿区信濃町35
慶應義塾大学医学部麻酔学教室

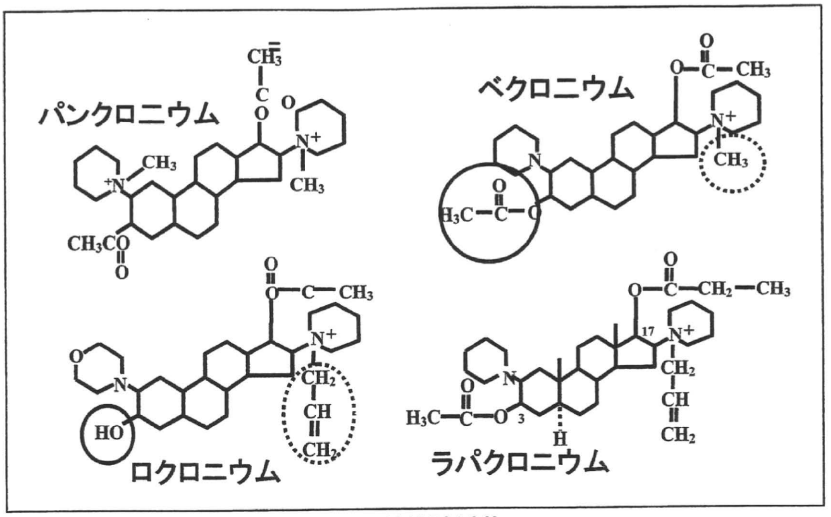

図1　アミノステロイド系非脱分極性筋弛緩薬
実線：ロクロニウムではA-ringの3位にOHが結合している．
破線：ベクロニウムのメチル基が，ロクロニウムではアリル基に変わる．

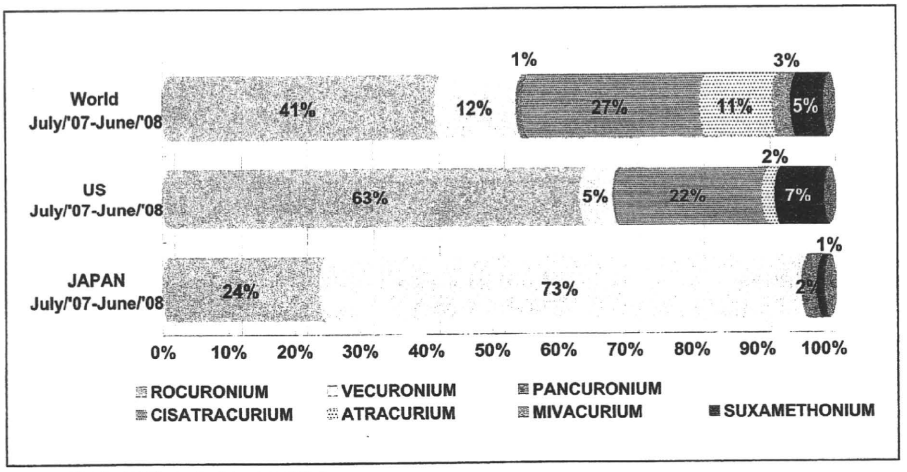

図2　筋弛緩薬の市場での割合

ロクロニウムは貯法として2～8℃に保存することが求められており，また薬事法での毒薬・劇薬の取扱いとして，“他の物と区別”することと，“かぎ”をかけての貯蔵が求められている．すなわち手術室内に鍵がかけられる冷暗所か冷蔵庫での貯蔵が義務となっており，使用上不便な点が欠点としてあげられる．

筋弛緩薬によるアナフィラキシー反応は，麻酔科医にとっては周知のことである．特にフランスでの報告例が多いことがよく知られている．Mertesら[1]の報告では，1999年から2000年までのフランスでのアナフィラキシー反応は，ロクロニウムでの発生が全体の43.1%，ベクロニウムでの発生が8.5%で，ロクロニウムでの発生率が高いという(**表1**)．発生率は使用頻度が高いと発生も多くなる可能性があるが，フランスでの使用頻度はロクロニウムが8.8%，ベクロニウムが11.3%で，ベクロニウムの使用頻度が高いにもかかわらず，アナフィラキシー反応の発生はロクロニウムの方が高かったという．Harboeら[2]の報告では，ノルウェーの1施設6年間での発

表1　アナフィラキシー(様)反応の発生率(フランス 1999-2000)

	Market Share* in Anesthesia (Vials), %	Anaphylactic Shocks 1999-2000	
		No.	%
Succinylcholine, 100mg/10ml	6.7	69	22.6
Rocuronium, 50mg/5ml	8.8	132	43.1
Rocuronium, 100mg/10ml			
Vecuronium, 4mg/1ml	11.3	26	8.5
Vecuronium, 10mg/1ml			
Pancuronium, 4mg/2ml	9.5	10	3.3
Atracurium	54.1	58	19.0
Atracurium, 50mg/5ml			
Mivacurium, 10mg/5ml	5.5	8	2.6
Mivacurium, 20mg/10ml			
Cisatracurium, 20mg/10ml	4.1	2	0.6
Cisatracurium, 5mg/2.5ml			
Cisatracurium, 10mg/5ml			
Gallamine, 40mg	—	1	0.3
Total		306	100

〔文献1)より引用〕

表2　ノルウェーの単施設，6年間のアナフィラキシー報告83例の原因物質

Causal Agent	Number of Cases (%)	Probable Causality	Possible Causality
All NMBAs	55(66.2)	45	10
Suxamethonium	30(36.1)	28	2
Rocuronium	17(20.5)	12	5
Vecuronium	6(7.2)	4	2
Pancuronium	1(1.2)	1	
Atracurium	1(1.2)		1
Latex	3(3.6)	3	
Hemaccel	1(1.2)		1
Unknown	24(28.9)		

〔文献2)より引用〕

生は，ベクロニウムの7.2%に比べて，ロクロニウムは20.5%と高かった(**表2**)．1999年から2002年までの文献を検索して検討したBhanankerら[3]の報告では，筋弛緩薬に対するアナフィラキシーの報告が少ない米国と，米国以外を比較したところ，ベクロニウムでは両者に差がなかったがロクロニウムでは有意に米国以外からの報告が多くみられた(**表3**)．

集中治療室でロクロニウムの繰り返しの投与や持続投与を行ったSparrら[4]の研究によると，ボーラスの繰り返し投与により筋弛緩を維持するには，最初の6〜9時間は多くの量が必要であるが，それ以降は減少して定常状態になる(**図3**)．また，ICUで平均40時間ロクロニウムの持続投与を行った場合の最終半減期は337±163分で，外科患者で使用した場

表3　アナフィラキシーの発生：文献検索(1999-2002)

Rocuronium				Vecuronium		
Preferred term (PT)	U.S. reports	Non-U.S. reports	P Value	Preferred term (PT)	U.S. reports	Non-U.S. reports
Anaphylactic reaction	1	11	<0.01	Anaphylactic reaction	5	5
Anaphylactic shock	22	59	<0.01	Anaphylactic shock	8	14
Anaphylactoid reaction	10	2	NS	Anaphylactoid reaction	7	4
Total reports with "anaphylaxis" term	33	72	<0.01	Total reports with "anaphylaxis" term	20	23
Total number of reports	166	145	—	Total number of reports	121	122

〔文献3)より引用〕

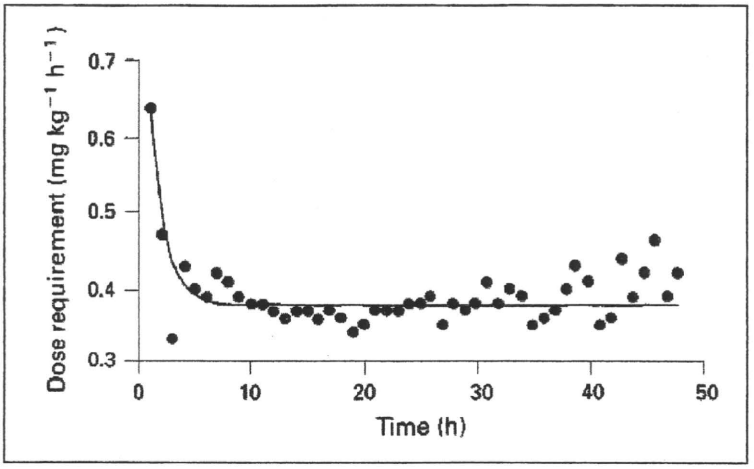

図3　ICUでのbolus投与により筋弛緩を維持するのに必要なロクロニウム量の経時的推移：27例の平均値

〔文献4)より引用〕

合の108±37分に比べ，大きく延長しており，長時間投与での作用延長の可能性が示唆されている(**表4**)．動物実験では，ラットに24時間投与して横隔膜の収縮力を検討したTestelmans[5]らの研究では，シスアトラクリウムに比べて収縮力が低下しており，筋のアトロフィの指標であるMURF-1が上昇しており(**図4**)，ロクロニウムによるMURF-1の上昇が筋収縮力の低下を引き起こしている可能性を示唆している．

小児への投与については，添付文書には「新生児に対する安全性は確立していない［使用経験が少ない．］．乳児，幼児，小児では慎重に投与すること［作用発現時間が早く，また小児では作用持続時間が短い．］．」と記載されている．Tobiasら[6]は，小児へのロクロニウムの投与で心拍数増加，血圧の上昇を報告しており，迷走神経遮断作用があること(**表5**)，また必要とする投与量が1日目の0.65g/kg/hに比べて，3日目には0.84g/kg/hに増加することから，耐性の可能性を指摘している．Playforら[7]のコンセンサスガイドラインでも，ベクロニウムには望ましくない作用が少ないことから，重症小児患者への筋弛緩薬投与では，持続注入ではベクロニウムを，間欠投与ではパンクロニウムを推奨しており，ロクロニウムは推奨されていない．以上のように，ロクロニ

表4 ICU患者と外科患者でのロクロニウムの薬物動態の違い

	ICU patients (n=12)	Surgical patients (i.v. anaesthesia; n=7)*	Surgical patients (halothane anaesthesia; n=8)**
Median duration of rocuronium administration (h)	39.38	2.16	1.23
Median total dose (mg)	937.5	195.7	67.0
Cl (ml/kg/min)	3.16(1.15) [1.39-5.07]	4.50(1.95) [2.80-8.61]	3.30(0.77) [1.97-4.55]
V^c (ml/kg)	160(88) [40-291]	146(56) [71-238]	62(8) [48-71]
V^{ss} (ml/kg)	769(334) [314-1351]	310(80) [205-408]	213(40) [152-303]
MRT (min)	262(120) [89-460]	78(36) [41-132]	67(19) [47-97]
$T_{1/2}{}^{\beta}$ (min)	337(163) [125-686]	108(37) [64-163]	86(18) [54-109]

(mean(SD)[range]；unless otherwise stated). V^{ss}(ml/kg)=Volume of distribution at steady state；$T_{1/2}{}^{\beta}$(min)=terminal half-life；Cl(ml/kg/min)=clearance；MRT(min)=mean residence time

〔文献4)より引用・改変〕

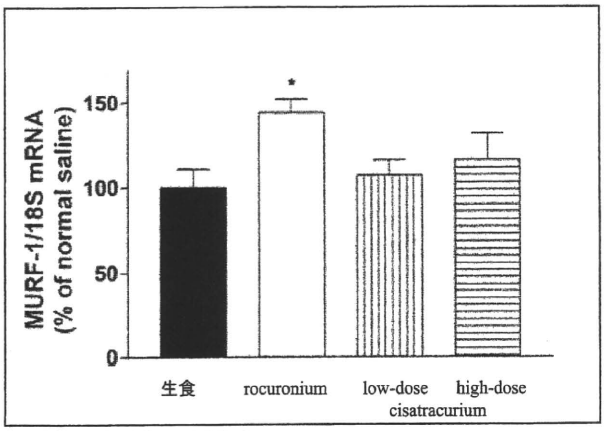

図4 筋弛緩薬の種類とMURF-1

〔文献5)より引用〕

ウムがすべての面でベクロニウムに勝っているわけではなく，ベクロニウムはまだ捨てがたいものがある．

Ⅱ スキサメトニウム

スキサメトニウムには，高カリウム血症，不整脈，頭蓋内圧亢進，胃内圧上昇，眼圧上昇，筋肉痛，悪性高熱症といった副作用があることが知られている．本邦では諸外国に比べてスキサメトニウムを特に嫌う文化があると考えられ，世界では筋弛緩薬の使用量の5%，米国では7%をスキサメトニウムが占めているのに比べて，日本では1%程度と極端に少ない(図2)．

一方，スキサメトニウムは，いずれの非脱分極性筋弛緩薬よりも速い作用発現，より十分な筋弛緩効果，短い作用持続時間，また胎児への移行がない，などの優れた特徴をもっており，いまだ筋弛緩薬のゴールドスタンダードとしての地位は譲ってはいない．スキサメトニウムの特徴から，現在も迅速導入(rapid sequence induction)，喉頭痙攣・麻薬によるrigidityへの対応時，挿管困難例，無痙攣性電気ショックの麻酔，日帰り麻酔，帝王切開術の麻酔などに使用されている．

通常使用量のスキサメトニウムの1mg/kgあるいはロクロニウムの0.6mg/kgを投与して挿管のしやすさを検討したCooperら[8]の報告では，スキサメトニウムでは投与60秒後，90秒後ともに“excellent”であったのに対して，ロクロニウムでは投与60秒後，90秒後ともに“good”や“fair”が存在しており，挿管状態はスキサメトニウムの方がよかったとしている．

Slugaら[9]は180名の緊急気管挿管を要する患者を対象に，プロポフォールで導入後，スキサメトニウム1mg/kgあるいはロクロニウム0.6mg/kgを投与して比較している．作用発現時間(図5)，挿管完了までの時間(図6)は有意にスキサメトニウムが短く，

表5　ロクロニウムの小児ICU患者14名での循環器系への影響

	Heart rate	Systolic BP	Diastolic BP
Baseline	121 ± 31	104 ± 28	62 ± 28
Maximum	132 ± 42*	112 ± 41 †	68 ± 36 †

*P<0.05 compared with baseline.
†P<0.01 compared with baseline.

〔文献6)より引用〕

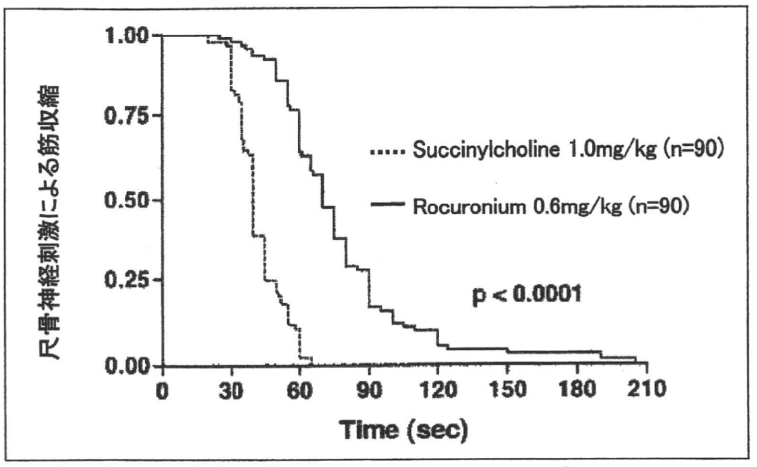

図5　迅速導入時の作用発現時間

〔文献9)より引用〕

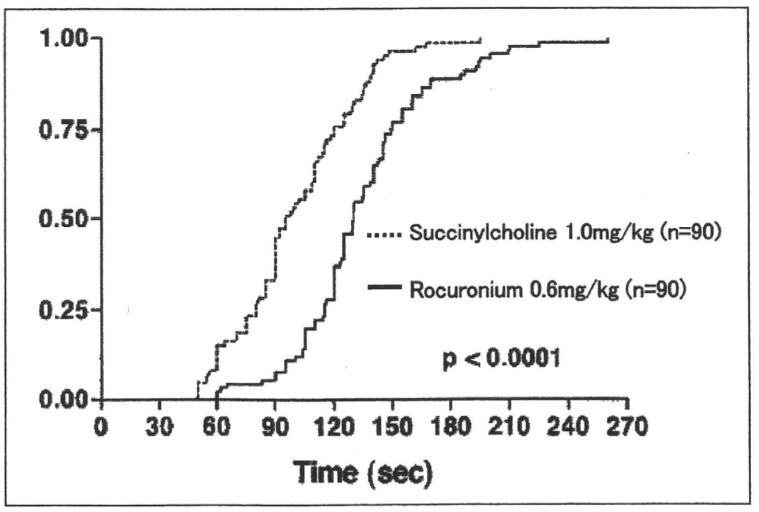

図6　迅速導入時の挿管完了までの時間

〔文献9)より引用〕

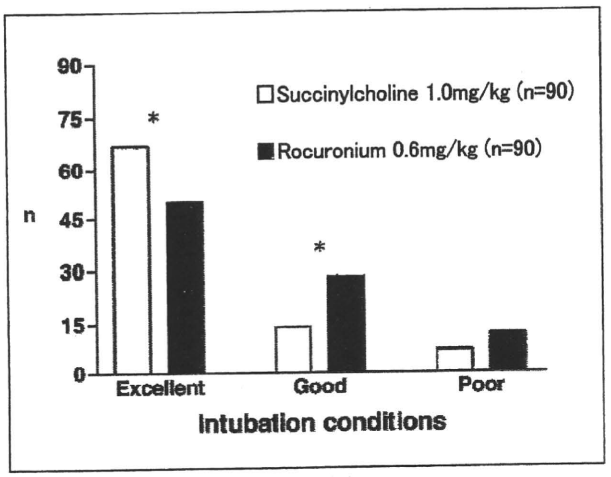

図7　迅速導入時の挿管の容易さ

〔文献9)より引用〕

挿管状態(図7)もスキサメトニウムの方が優れており，緊急の症例ではスキサメトニウムの方が優れていると結論づけている．

Cochraneデータベースでは，迅速導入時に使用する筋弛緩薬について，2003年にはロクロニウムはスキサメトニウムより劣ってはいるが，プロポフォールによる導入を行えば，挿管状態は同じとしていたが[10]，さらに例数を増やしての2008年の報告では，スキサメトニウムの方がロクロニウムより勝っており，麻酔導入にプロポフォールを用いたときでもスキサメトニウムの方が優れていると変わっている[11]．同様に喉頭痙攣や麻薬によるrigidityの発生時の緊急対応には，スキサメトニウムの方が優れている．

帝王切開術の麻酔は，脊髄くも膜下麻酔が一般的に行われているが，全身麻酔を必要とするときもある．全身麻酔による帝王切開術の導入は，迅速導入に準じて行われ，『ミラー麻酔科学』[12]では「帝王切開を全身麻酔で行う場合の推奨される方法」として，「チオペンタール4～5mg/kgに，スキサメトニウム1～1.5mg/kgで迅速導入を行う.」としている．“Clinical Anesthesiology”[13]でも，帝王切開時の推奨される麻酔法として，「プロポフォール2mg/kgかチオペンタール4mg/kgにスキサメトニウム1.5mg/kgを用いて迅速導入を行う.」としており，作用発現が速く，良好な筋弛緩状態が得られ，挿管困難であっても筋弛緩作用持続は短時間のスキサメトニウムが基本となっている．

スキサメトニウムは他の筋弛緩薬にはない大きな特徴をもっており，臨床での使用価値は高く，また緊急時対策として常備している施設も少なくないことから，スキサメトニウムもまだまだ捨てがたい筋弛緩薬といえる．

本稿の要旨は日本臨床麻酔学会第28回大会(2008，京都)パネルディスカッション(2)「ディベイト・神経筋遮断薬」において発表した．

参考文献

1) Mertes PM, Laxenaire MC, Alla F : Anaphylactic and anaphylactoid reactions occurring during anesthesia in France in 1999-2000. Anesthesiology 99 : 536-545, 2003
2) Harboe T, Guttormsen AB, Irgens A, et al. : Anaphylaxis during anesthesia in Norway : a 6-year single-center follow-up study. Anesthesiology 102 : 897-903, 2005
3) Bhananker SM, O'Donnell JT, Salemi JR, et al. : The risk of anaphylactic reactions to rocuronium in the United States is comparable to that of vecuronium : an analysis of food and drug administration reporting of adverse events. Anesth Analg 101 : 819-822, 2005
4) Sparr HJ, Wierda JM, Proost JH, et al. : Pharmacodynamics and pharmacokinetics of rocuronium in intensive care patients. Br J Anaesth 78 : 267-273, 1997
5) Testelmans D, Maes K, Wouters P, et al. : Infusions of rocuronium and cisatracurium exert different effects on rat diaphragm function. Intensive Care Med 33 : 872-879, 2007
6) Tobias JD : Continuous infusion of rocuronium in a paediatric intensive care unit. Can J Anaesth 43 : 353-357, 1996
7) Playfor S, Jenkins I, Boyles C, et al. : Consensus guidelines for sustained neuromuscular blockade in critically ill children. Paediatr Anaesth 17 : 881-887, 2007
8) Cooper R, Mirakhur RK, Clarke RS, et al. : Comparison of intubating conditions after administration of Org 9246 (rocuronium) and suxamethonium. Br J Anaesth 69 : 269-273, 1992

9) Sluga M, Ummenhofer W, Studer W, et al. : Rocuronium versus succinylcholine for rapid sequence induction of anesthesia and endotracheal intubation : a prospective, randomized trial in emergent cases. Anesth Analg 101 : 1356-1361, 2005
10) Perry J, Lee J, Wells G : Rocuronium versus succinylcholine for rapid sequence induction intubation. Cochrane Database Syst Rev 2003(1) : CD002788
11) Perry JJ, Lee JS, Sillberg VA, et al. : Rocuronium versus succinylcholine for rapid sequence induction intubation. Cochrane Database Syst Rev 2008(2) : CD002788
12) Birnbach DJ, Browne IM : 産科麻酔, ミラー麻酔科学. Miller RD編, 武田純三監修. メディカル・サイエンス・インターナショナル, 東京, 2007, 1791-1822
13) Morgan GE, et al.(ed) : Obstetric anesthesia, Clinical Anesthesiology, 4th ed. Lange Medical Books, McGraw-Hill, New York, 2006, 890-921

Vecuronium and Suxamethonium are also Useful Neuromuscular Blocking Agents, in Addition to Rocuronium

Junzo TAKEDA

Department of Anesthesiology, School of Medicine, Keio University

Rocuronium became available on the market in 2007 in Japan, and it was about ten years behind the rest of the world. The use of rocuronium is increasing quickly in Japan. However, vecuronium and suxamethonium are still being used in the world now. Rocuronium has outstanding features such as rapid onset and, no accumulation, and it comes in the form of a ready-to-use solution, but it has a similar duration to vecuronium, a higher risk of anaphylactic reactions, possible accumulation by long-term injection in patients in intensive care, and few data in pediatric patients. Suxamethonium is superior as a neuromuscular blocking agent in rapid sequence induction, in anesthesia for cesarean section and in emergency situations. It could still be considered that vecuronium and suxamethonium are also useful agents, in addition to rocuronium.

Key Words : Rocuronium, Vecuronium, Suxamethonium, Anaphylactic reactions, Rapid sequence induction

Autophagy 6:3, 378-385; April 1, 2010; © 2010 Landes Bioscience

Dynein- and activity-dependent retrograde transport of autophagosomes in neuronal axons

Kiyoshi Katsumata,[1,2] Jun Nishiyama,[1] Takafumi Inoue,[3] Noboru Mizushima,[4] Junzo Takeda[2] and Michisuke Yuzaki[1,*]

[1]Department of Neurophysiology; [2]Department of Anesthesiology; School of Medicine; Keio University; Tokyo, Japan; [3]Department of Life Science and Medical Bioscience; Waseda University; [4]Department of Cellular Physiology; Tokyo Medical and Dental University; Tokyo, Japan

Key words: autophagosome, cerebellum, granule cell, imaging, EHNA, NMDA

Abbreviations: *Atg*, autophagy-related genes; PBS, phosphate-buffered saline; P, postnatal day; NMDA, *N*-methyl-*D*-aspartic acid; APV, D-2-amino-5-phosphono-valeric acid; EHNA, erythro-9-[3-(2-hydroxynonyl)] adenine; BafA, bafilomycin A1

The accumulation of autophagosomes within axons is often observed in axonopathies associated with various neurological disorders, including those following excitotoxic insults. Nevertheless, the life cycle of autophagosomes in axons is not well understood. In the present study, we used microexplant cultures of cerebellar granule cells from *GFP-LC3* transgenic mice to perform time-lapse imaging of LC3-positive dots in identified axons. Since these GFP-LC3 dots were never observed in granule cells on an *Atg5*-null background, they were considered to represent autophagosomes. Under physiological conditions, the autophagosomes showed bidirectional and saltatory movement with a bias towards one direction. Such vectorial movement was largely blocked by the dynein motor inhibitor EHNA (erythro-9-[3-(2-hydroxynonyl)] adenine), suggesting that the autophagosomes moved towards the soma, where most lysosomes are located. Interestingly, the application of the glutamate analog *N*-methyl-*D*-aspartic acid (NMDA) as an excitotoxin increased the number of autophagosomes in axons, while it did not significantly change its movement characteristics. These results suggest that autophagosomes play important roles in axons and are dynamically regulated under physiological and pathological conditions.

Introduction

Macroautophagy (which we will refer to as autophagy hereafter) is a regulated catabolic mechanism whereby cells degrade their own proteins and organelles in response to nutrient starvation.[1] Many autophagy-related genes (*Atg*) have been identified in yeast, and most of these genes are thought to play similar roles in mammalian cells.[2] Two ubiquitin-like systems, the *Atg12* and *Atg8* (*LC3* in mammals) systems, are crucial for autophagy; mice deficient for *Atg5* or *Atg7*, both of which are necessary for the *Atg12* and/or *Atg8* conjugation systems, die during neonatal periods of starvation because of a lack of autophagy.[3,4] Although the basal level of autophagic activity is relatively low in the brain, the neuron-specific knockout of *Atg5* or *Atg7* results in a slow neurodegeneration in a cell-autonomous manner.[5,6] Interestingly, the first sign of neurodegeneration in these mice is the accumulation of aberrant membrane structures in swollen axons,[7,8] indicating that the autophagic pathway serves unidentified but important physiological functions within axons. Although whether the autophagic pathway exerts anti- or pro-death roles in neurons under pathological conditions remains unclear,[9] the accumulation of autophagosomes within axons is often associated with various neurodegenerative disorders,[10,11] such as Alzheimer disease,[12] Huntington disease,[13] Parkinson disease[14] and excitotoxic rodent models.[15,16] Despite the potential importance of autophagy in axons, the entire life cycle of autophagosomes in axons is not well understood; how autophagosomes are trafficked and fuse with lysosomes, which are mainly located in cell bodies distant from the axons, remains largely unclear.

Recently, taking advantage of green fluorescent protein (GFP)-labeled LC3 as a reliable marker of autophagosomes,[17] the life cycle of autophagosome has begun to be characterized using real-time imaging in neurons and neuronal cell lines. In primary superior cervical ganglion (SCG) neurons and PC12 cells, autophagosomes were initially observed in neurites but then underwent retrograde and antegrade transport to the cell body following nutrient deprivation.[18] In contrast, a preliminary report showed that GFP-LC3 underwent retrograde transport in the axons of cerebellar granule neurons in dissociated cultures.[19] One confounding factor in these studies may be the inclusion of both dendrites and axons in these analyses, since it is often difficult to differentiate axons from dendrites on the basis of morphology alone. In addition, the CNS axons, which extend for a long distance, are considerably different from the axons of PNS and PC12 cells. Furthermore, when transiently overexpressed, GFP-LC3 can be incorporated into protein aggregates independent of autophagy.[20] To circumvent these problems in the present study, we adopted microexplant cultures of newborn mouse

*Correspondence to: Michisuke Yuzaki; Email: myuzaki@a5.keio.jp
Submitted: 11/09/09; Revised: 01/19/10; Accepted: 01/20/10
Previously published online: www.landesbioscience.com/journals/autophagy/article/11262

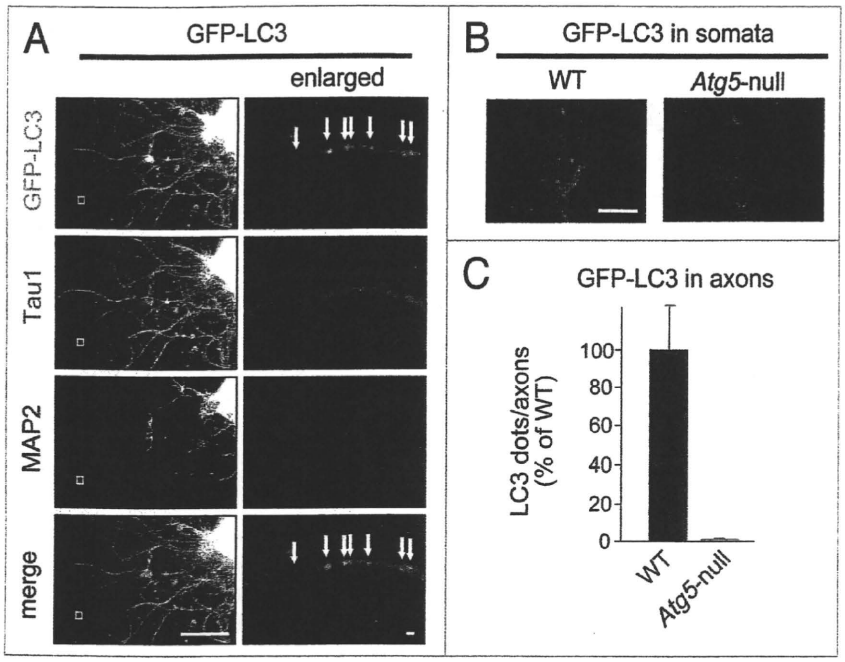

Figure 1. LC3-positive autophagosomes in the axons of granule cells in microexplant cultures. (A) Immunostaining of microexplant cultures prepared from *GFP-LC3* transgenic mice on postnatal day 8. The cultures were fixed at 8 days in vitro and immunostained for an axonal marker tau-1 (blue) and a dendritic marker MAP2 (red). Long and thin neurites in the region distant from the microexplant core were considered axons as they were immunopositive for tau-1 but immunonegative for MAP2. The axons shown in the white boxes on the left panels are enlarged in the right panels. The white arrows indicate the GFP-LC3 dots in the axons. Scale bars, 50 μm (left), 1 μm (right). (B) Absence of GFP-LC3 dots in the soma of *Atg5*-null granule cells. Representative images of granule cells prepared from *GFP-LC3* (left) and *GFP-LC3*; *Atg5*$^{flox/flox}$; *nestin-Cre* (right) mice are shown. Scale bar, 10 μm. (C) Absence of GFP-LC3 dots in the axons of *Atg5*-null granule cells. The total number of GFP-LC3 dots was counted in 10-μm lengths randomly selected on at least 10 axons from three independent cultures for wild-type and *Atg5*$^{flox/flox}$; *nestin-Cre* mice.

cerebellar cortex, in which the granule cells migrate with easily identified axons. In addition, by preparing the cultures from *GFP-LC3* transgenic mice, we were able to monitor the autophagosomes and their kinetics in the granule cell axons in a reliable manner. Under physiological conditions, we found that autophagosomes moved in a salutatory manner; that is, they moved and stopped repeatedly, and sometimes changed direction, with a bias towards one direction. This vectorial movement was dependent on a dynein motor. Although the application of the glutamate analog *N*-methyl-*D*-aspartic acid (NMDA) as an excitotoxin increased the number of autophagosomes in the axons, it did not significantly change their movement characteristics.

Results

In vitro model for monitoring the dynamics of autophagosomes in neuronal axons. To monitor the dynamics of autophagosomes in the axons of homogenous CNS neurons, we utilized cerebellar microexplant cultures, in which almost all the neurons are granule cells that differentiate synchronously in vitro.[21] In addition, the granule cells reportedly migrate from microexplants, guided by a leading process that later forms a parallel fiber axon in vitro.[22] First, we immunostained microexplant cultures prepared from *GFP-LC3* transgenic mice on postnatal day 7–8 (P7-8) using an axonal marker, tau-1, and a dendritic marker, microtubule-associated protein 2 (MAP2), at 7 d in vitro (DIV). Consistent with the findings of earlier studies,[23] long and thin neurites formed bundles, which were always immunopositive for tau-1 but immunonegative for MAP2 in the region distant from the microexplant core, whereas a small portion of short tangential neurites near the microexplant core were immunopositive for MAP2 (**Fig. 1A**). We observed a small number of GFP-LC3 puncta within the axons (**Fig. 1A**) and soma (**Fig. 1B**) of the granule cells under normal (without nutrient deprivation) conditions. This finding is consistent with earlier reports that the basal autophagic activity is low in neurons.[5,6] To confirm that the GFP-LC3 dots represent autophagosomes, we prepared cultures from neuron-specific *Atg5* knockout mice expressing GFP-LC3 by crossing *GFP-LC3* transgenic mice with *Atg5*$^{flox/flox}$; *nestin-Cre* mice.[5] As expected, small GFP-LC3 puncta were essentially missing in the soma (**Fig. 1B**) and axons (**Fig. 1C**) of granule cells in microexplant cultures prepared from *GFP-LC3*; *Atg5*$^{flox/flox}$; nestin-*Cre* transgenic mice. Although rare, relatively large and high-intensity GFP-LC3 dots, which appear to be protein aggregates, were observed in the soma of a few *GFP-LC3*; *Atg5*$^{flox/flox}$; nestin-*Cre* neurons. Similar GFP-LC3 dots, which were immunopositive for ubiquitin, were observed in some neurons of *GFP-LC3*; *Atg5*$^{-/-}$ neonates.[5] Taken together, these results indicate that small GFP-LC3 dots observed in microexplant granule cell cultures correspond to autophagosomes and that this system serves as a good model for analyzing autophagosomes in axons.

Dynamics of autophagosomes in axons. We next performed time-lapse imaging of the GFP-LC3 autophagosomes within the axons of granule cells using microexplant cultures. To follow the movement of the autophagosomes while minimizing phototoxicity and photobleaching, we took images every 10 s for a total duration of 5 min (**Fig. 2A, Suppl. movie**). To analyze the dynamics of the movements, we constructed a kymograph by plotting the position of each autophagosome as a function of time; the initial and final positions of each autophagosome were defined as zero and positive, respectively (**Fig. 2B**). Interestingly, while some GFP-LC3 autophagosomes moved continuously during the observation period (blue arrowheads, **Fig. 2B**), others stopped after their initial movement (blue arrows) or moved in a salutatory manner (orange arrowheads). Furthermore, the autophagosomes occasionally moved in a direction opposite to that of the final destination (red arrows, **Fig. 2B**). The distance that each autophagosome traveled in each 10-s frame ranged from ~2.0 μm

to +4.9 μm, with an average of 0.50 ± 0.03 μm (mean ± SEM, n = 840 frames; **Fig. 2C**). The maximal speed at which each autophagosome moved during the 5-min observation period ranged from 0.07 μm/s to 0.49 μm/s, with an average of 0.25 ± 0.02 μm/s (mean ± SEM, n = 28; **Fig. 2D**). These results indicate that the autophagosomes observed in axons are not static, but that they move dynamically by changing speeds and sometimes directions.

Dynein-dependent retrograde transport of autophagosomes in axons. Although the autophagosomes moved bidirectionally, they preferentially moved in one direction (**Fig. 2B and C**). However, it was impossible to determine the preferential direction using time-lapse imaging because the movement of single autophagosomes could not be followed near the center of the microexplants, from which many of the axons emerged. The retrograde transport of vesicles and many organelles in axons towards the nucleus is known to depend on the motor protein dynein, which moves along microtubules to its minus ends. Thus, to examine the direction and the motor responsible for the movement of autophagosomes in axons, we treated microexplant cultures with a dynein ATPase inhibitor, erythro-9-[3-(2-hydroxynonyl)] adenine (EHNA; 50 μM),[24] for 4 h, which reportedly has little effect on the antegrade axonal transport.[25] The kymographic analysis indicated that this treatment significantly reduced the movement of the autophagosomes in the axons (**Fig. 3A**). The mean distance that the autophagosomes moved during the 5-min observation periods was significantly shorter in cultures treated with EHNA (4.3 ± 0.53 μm, n = 26) than in those treated with DMSO (15.1 ± 1.7 μm, n = 28; $p < 0.01$ according to the Mann-Whitney *U* test; **Fig. 3B**). Similarly, the maximal speed at which each autophagosome moved during the 5-min observation was significantly slower in cultures treated with EHNA (0.13 ± 0.02 μm) than in those treated with DMSO (0.25 ± 0.02 μm; $p < 0.01$ according to the Mann-Whitney *U* test; **Fig. 3C**). EHNA treatment did not inhibit the movement of DsRed-tagged synaptophysin, which is mainly transported by antegrade motors in the axons (**Fig. 3D**), confirming the specific effects of EHNA on retrograde motors. Autophagosomes are known to target lysosomes, where their contents are degraded. As reported earlier,[12,26] the lysosomal marker lamp-1 was virtually missing in axons and was localized mainly in the soma, partially overlapping with the GFP-LC3 dots (**Fig. 3E**). Altogether, these results indicated that although the autophagosomes moved bidirectionally in axons, they traveled preferentially in a retrograde direction via dynein motors to the neuronal cell body, where the lysosomes are located. Although dynein may also be involved in the fusion between autophagosomes and lysosomes, its major role in axons is likely retrograde transport of autophagosomes back to the cell body where lysosomes were mainly located.

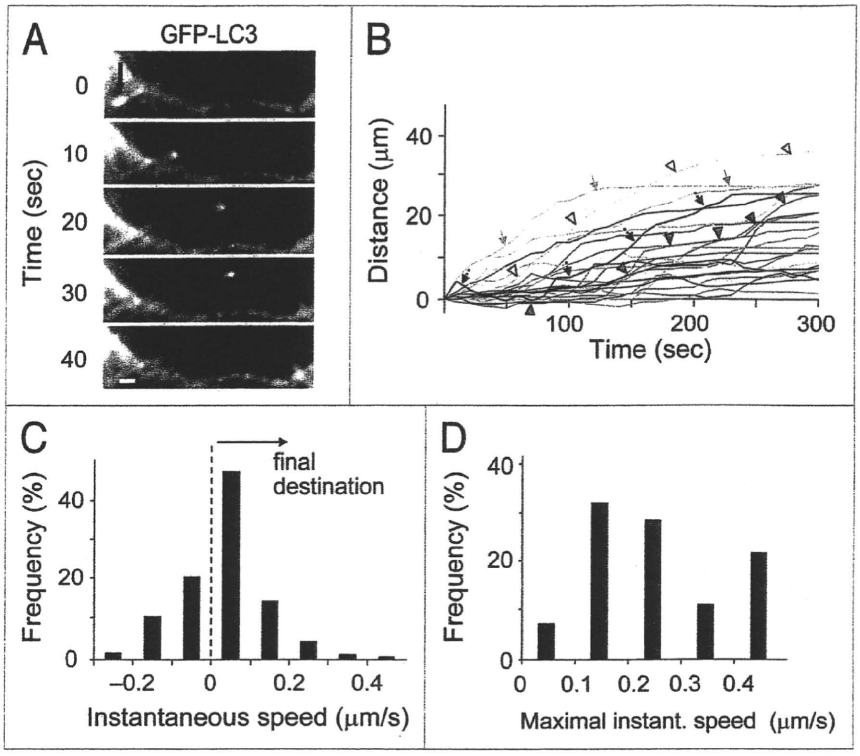

Figure 2. Movement of LC3-positive autophagosomes in axons. (A) Representative time-lapse images of GFP-LC3 dots in axons of granule cells. The arrows indicate autophagosomes moving along the axons of *GFP-LC3* granule cells in microexplant cultures. Scale bar, 1 μm. (B) Kymographs of autophagosomes in axons. The positions of 28 autophagosomes in the axons of *GFP-LC3* granule cells were recorded every 10 s and plotted against time. The initial and final positions of each autophagosome were defined as zero and positive, respectively. Several movement patterns of the autophagosomes are shown by the arrows and arrowheads (see Results). The interval between the time-lapse image frames was 10 s. (C) Frequency histogram of the instantaneous speed of each autophagosome per frame. The instantaneous speed was measured by dividing the distance that each autophagosome traveled per 10-s frame and was plotted as a histogram of the occurrence. The arrow indicates the final direction of the movement; the frequency distribution was skewed towards this direction. (D) Frequency histogram of the maximal instantaneous speed of autophagosomes per frame. The maximal instantaneous speed at which each autophagosome moved during the 5-min observation period was plotted as a histogram of the occurrence.

Neuronal activity-dependent change in the kinetics of autophagosomes in neuronal axons. The accumulation of autophagosomes within axons has been reported in various neurodegenerative disorders, which are associated with excitotoxicity.[10,11] Thus, we next investigated the effect of NMDA treatment on the dynamics of autophagosomes in axons. Microexplant cultures were incubated in a medium containing 300 μM of NMDA plus 5 μM of glycine or the selective NMDA antagonist *D*-2-amino-5-phosphonovaleric acid (APV; 50 μM) as a control for 24 h. Under these conditions, the lactose dehydrogenase (LDH) levels increased in the NMDA-treated cultures (11 ± 2% of total LDH content, n = 4) to a greater extent than in the control cultures (4.0 ± 0.1% of total LDH content, n = 4; $p < 0.01$ according to the Student's t test). Similarly, the number of GFP-LC3 dots increased by approximately 2.5-fold in the axons of NMDA-

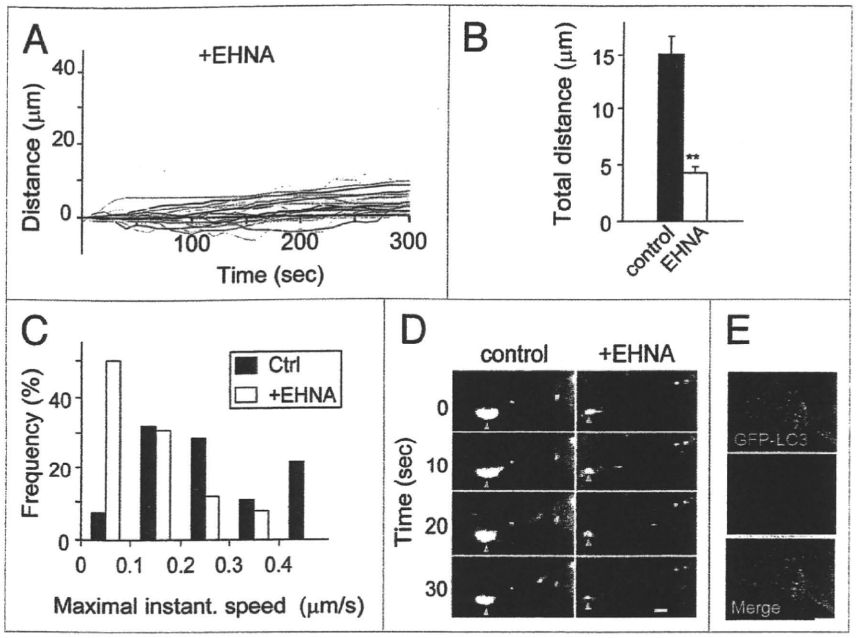

Figure 3. EHNA treatment inhibited the movement of autophagosomes in axons. (A) Kymographs of autophagosomes following EHNA treatment. After treating the GFP-LC3 granule cells with EHNA (50 μM) for 4 h, the positions of 26 autophagosomes in the axons were recorded every 10 s and plotted against time. (B) Total distance that the autophagosomes travelled in control and EHNA-treated granule cell axons during 5-min periods. (C) Frequency histogram of the maximal instantaneous speed of autophagosomes per frame. The maximal instantaneous speed at which each autophagosome moved during the 5-min observation period in control and EHNA-treated granule cell axons was plotted. **$p < 0.01$. (D) Representative time-lapse images of DsRed-tagged synaptophysin in axons of granule cells. Cerebellar explant cultures were infected with lentivirus encoding DsRed-synaptophysin at 7 DIV and imaged at 14 DIV after treatment with or without EHNA for 4 h. Red arrows indicate DsRed-synaptophysin fluorescence and blue arrowheads indicate synaptic buttons. Scale bar, 1 μm. (E) Colocalization of GFP-LC3 dots with putative lysosomes in the soma of granule cells. *GFP-LC3* granule cells were fixed and double-immunostained for a lysosomal marker lamp-1 (red) and GFP-LC3 (green).

treated granule neurons ($p < 0.01$ according to the Mann Whitney *U* test; **Fig. 4A**). Time-lapse imaging of the GFP-LC3 dots in the axons revealed that the population of fast-moving autophagosomes tended to increase in the axons of NMDA-treated neurons (**Fig. 4B**), although most autophagosomes moved relatively slowly in both NMDA-treated and control neurons; thus, the mean distances that the autophagosomes traveled did not differ significantly between these two groups (**Fig. 4C**). Similarly, the maximal speed at which each autophagosome moved during the 5-min observation periods peaked at 0.4–0.5 μm/s in neurons treated with NMDA, while it peaked at 0.2–0.3 μm/s in the control neurons (**Fig. 4D**), although the mean velocity did not differ significantly between these two groups (0.36 ± 0.03 μm/s for NMDA vs. 0.27 ± 0.03 μm/s for control, $p > 0.1$ according to the Mann-Whitney *U* test). Thus, although whether NMDA treatment increased the overall trafficking of autophagosomes remains unclear, it seemed to stimulate the movement of at least a proportion of the autophagosome population. These results indicate that excitotoxic stimuli, as mimicked by NMDA treatment, increased the number of autophagosomes in axons not by inhibiting their movements.

Finally, to further examine whether NMDA treatment increased the de novo formation of autophagosomes, we performed immunoblotting analysis with anti-LC3 antibody; a lipidated form of LC3, LC3-II, has been shown to be a specific autophagosomal marker in mammals.[27] We found that the ratio of LC3-II to its unlipidated form LC3-I was significantly increased in lysates prepared from cultured granule cells treated with 300 μM of NMDA plus 5 μM of glycine for 24 h ($p < 0.05$, $n = 5$; **Fig. 5A and B**). When fusion of autophagosomes and lysosomes was blocked by incubation with a medium containing 200 nM of bafilomycin A1 (BafA)[28] for the last 4 h, the LC3-II/LC3-I ratio was significantly increased in both control and NMDA-treated granule cells ($p < 0.01$ vs. control without BafA, $n = 5$; **Fig. 5A and B**). Importantly, the LC3-II/LC3-I ratio was significantly higher in NMDA/BafA-treated cells than in NMDA-treated cells ($p < 0.01$, $n = 5$; **Fig. 5A and B**), a result indicating that NMDA-induced increase in the LC3-II/LC3-I ratio was caused by enhancement of the autophagic influx, not by inhibition of autophagic degradation.[29,30] Furthermore, the level of p62/SQSTM1, a selective substrate of autophagy used as an indicator of autophagic degradation activity,[31] was reduced by NMDA treatment (**Fig. 5C**). These results are consistent with increased GFP-LC3 dots in axons of granule cells (**Fig. 4**) and support the view that NMDA treatment increased the de novo formation of autophagosomes in granule cells.

Discussion

Although the accumulation of autophagosomes within axons is often observed in axonopathies associated with various neurological disorders, the life cycle of autophagosomes in axons is not well understood.[10,11] In the present study, we used microexplant cultures of cerebellar granule cells from GFP-LC3 transgenic mice to perform time-lapse imaging of LC3-positive autophagosomes in well-defined CNS axons.

Dynamics of autophagosomes in axons under physiological conditions. The basal autophagic activity level is generally considered very low in the brain in vivo.[5,6] Nevertheless, we constantly observed a small number of GFP-LC3 dots in the axons of cultured granule cells under normal conditions. This result might be explained by the difficulty that arises when using the thin slices required for an electron microscopic analysis to detect the small number of autophagosomes in long axons running in various directions. In addition, since the granule cells that were used in this study correspond to those at early developmental stages (postnatal days 10–14), the endogenous autophagic activity level might have been relatively high.[32] Also, the autophagic

activity level might have been somewhat increased because of the culture conditions, under which some nutrients were missing. Nevertheless, few autophagosome-like double membrane structures have been reported in the axons of wild-type Purkinje cells neurons in vivo.[7,33] In addition, the earliest sign of neurodegeneration in neuron-specific *Atg5* or *Atg7* knockout mice is a local swelling of the axons around their terminals,[7,8] indicating that autophagic activity plays crucial physiological roles in the maintenance of axons. Therefore, we believe that the dynamics of autophagosomes observed in cultured granule cells at least partly reflect those naturally occurring in vivo.

Microtubules are arranged in axons so that each minus end points toward the nucleus. Dynein is the major minus-end motor that transports various cargos on microtubules. Since the movement of the autophagosomes in the axons was greatly reduced by the dynein motor inhibitor EHNA (**Fig. 3A–C**), the autophagosomes likely traveled preferentially in a retrograde direction via dynein motors. Autophagosomes were previously reported to undergo bidirectional transport in neurites following the deprivation of a nerve growth factor in SCG neurons and PC12 cells.[18] The reason why autophagosomes did not show vectorial movement in neurites (a mixture of axons and dendrites) of SCG neurons and PC12 cells is unclear, but microtubules may be arranged differently in neurites than in axons. In contrast, GFP-LC3 reportedly exhibited unidirectional, retrograde transport in putative axons of cerebellar granule cells in dissociated cultures when examined in a preliminary study.[19] Although the details were not described, small antegrade movement could be easily missed if time-lapse imaging was performed for a short duration or at long intervals. Recently, autophagosomes have been shown to travel bidirectionally with a net movement towards the microtubule-organizing center in HeLa cells[34] and rat kidney cells.[35] Furthermore, the movement of autophagosomes and its fusion with lysosomes, which are located around the centrosome, was also reduced by EHNA and other reagents blocking dynein motors in these cells.[34,35] Therefore, the present study has not only confirmed earlier studies reporting that autophagosomes show dynamic movements in neurons, but has also established the view that autophagosomes undergo bidirectional transport with a bias towards the soma, where most lysosomes are located (**Fig. 3D**), in the CNS axons as well as in other non-neuronal cells.

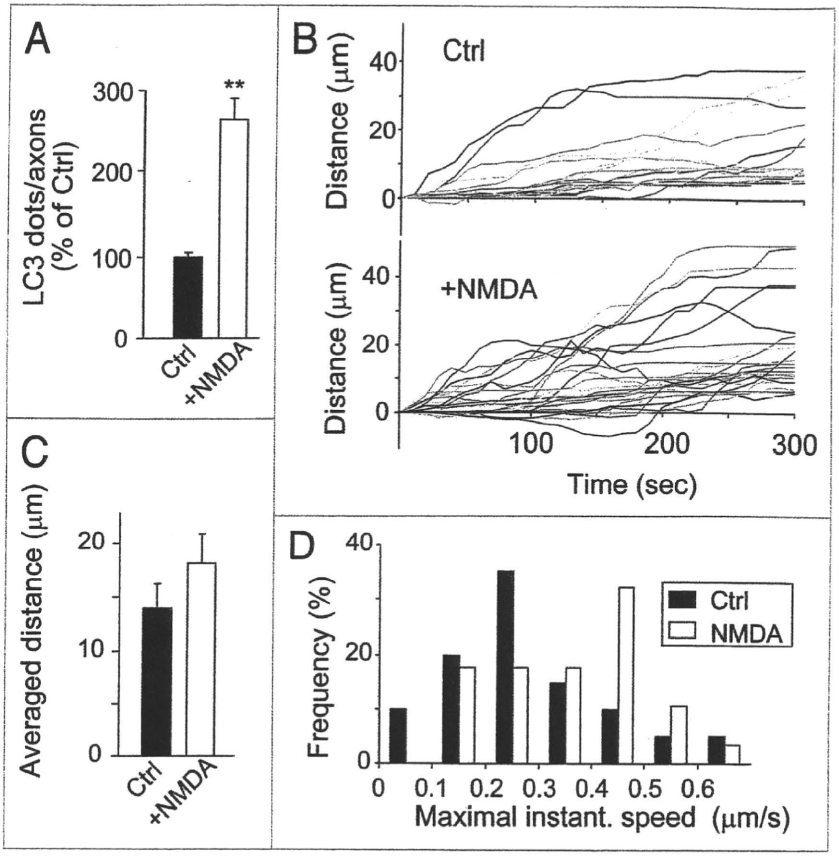

Figure 4. Activity-dependent regulation of autophagosomes in granule cell axons. (A) Increased number of autophagosomes in the axons of granule cells treated with NMDA. The number of GFP-LC3 dots per unit length in randomly selected distal axons was counted in granule cells treated with NMDA (300 μM) plus glycine (5 μM) for 24 h. The value in control granule cells treated with APV (50 μM) was arbitrarily defined as 100%. **$p < 0.01$, $n = 30$ regions each. (B) Kymographs of autophagosomes in control and NMDA-treated granule cells. After treating GFP-LC3 granule cells with NMDA or APV (control) for 24 h, the positions of the autophagosomes (26 for control and 28 for NMDA) in the axons were recorded every 10 s and plotted against time. (C) Total distance that the autophagosomes traveled in control and NMDA-treated granule cell axons during 5-min periods. (D) Frequency histogram of the maximal instantaneous speed of autophagosomes per frame. The maximal instantaneous speed at which each autophagosome moved during the 5-min observation period in control and NMDA-treated granule cell axons was plotted.

Autophagosomes under pathological conditions. The application of NMDA[15,16] or kainate[36] to neurons reportedly results in an increase in the number of autophagosome-like structures and the accumulation of the lipidated form of LC3, which is associated with autophagosomal membranes, in neurons. Although the mechanisms underlying this phenomenon are still unclear, either an enhancement in the de novo formation of autophagosomes or a decrease in the clearance of existing autophagosomes might be responsible. For example, the decreased clearance of autophagosomes is associated with several neurodegenerative disorders, such as Alzheimer disease[12] and Parkinson disease.[14] In contrast, in *lurcher* mutant mice, where a constitutive activity of the δ2 glutamate receptor causes the neurodegeneration of cerebellar Purkinje cells,[37,38] the earliest sign of abnormality was the accumulation of autophagosomes in Purkinje cell axons without a reduction in the clearance of autophagosomes.[39] Recently, autophagosome formation in *lurcher* have been shown to be caused by excessive cation influx into Purrkinje cells.[40] The present findings that NMDA treatment increased the number of GFP-LC3 dots in axons (**Fig. 4**) and enhanced the de novo formation of autophagosomes (**Fig. 5**) also support the view that

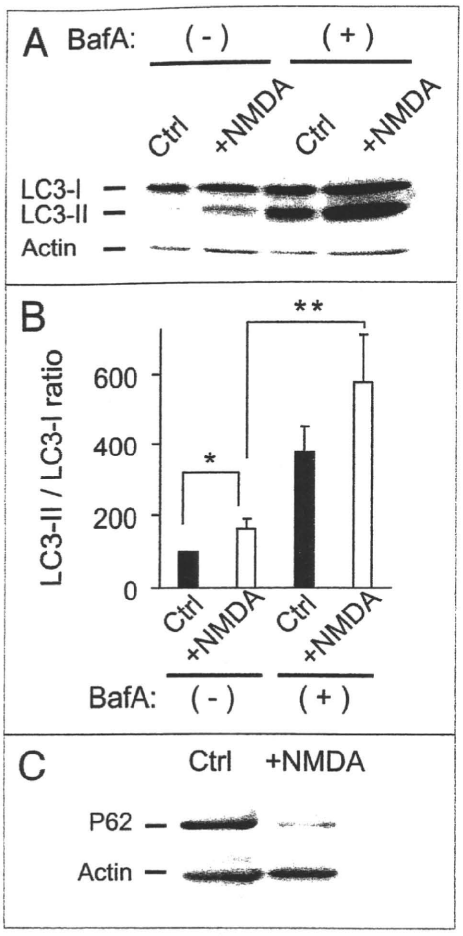

Figure 5. The effect of NMDA treatment on the production and degradation of autophagosomes. (A and B) Cultured granule cells were treated with 50 μM APV (Ctrl) or 300 μM NMDA plus 5 μM glycine (+NMDA) for 24 h. The cells were treated with (+) or without (-) 200 nM bafilomycin A1 (BafA) for the last 4 h and subjected to immunoblot analysis using anti-LC3 and anti-actin antibodies. Representative images (A) and quantitative analysis (B) were shown. The actin level was shown as a control. Each bar represents the mean + SEM (n = 5) *p < 0.05, **p < 0.01. (C) Immunoblot analysis of granule cells treated with NMDA using anti-p62/SQSTM1 antibody. The p62/SQSTM1 level was reduced in granule cells treated with 300 μM NMDA plus 5 μM glycine (+NMDA) for 24 h, a result indicating an increased autophagic activity. The actin level was shown as a control.

excitotoxic insults, which accompany cation influx, induce the formation of autophagosomes in axons.

Although the maximal movement of the autophagosomes in the axons (0.07–0.49 μm/s; **Fig. 2D**) was slower than what can be achieved using dynein motors (1–4 μm/s),[41] it was similar to that observed in rat kidney cells (0.05–0.24 μm/s).[35] Similarly, although the responsible motors are unclear, ER subcompartments and RNA granules have been shown to travel bidirectionally in the dendrites of hippocampal neurons at speeds of 0.2–0.3 μm/s.[42] The slow movement of autophagosomes observed in axons may result from the occurrence of intermittent pauses or directional switching. Thus, if the formation of autophagy is further increased under pathological conditions in neurons that have long axons, the slow speed of the retrograde movement could become the rate-limiting step of the turnover of autophagosomes. Indeed, the loss of dynein function reportedly causes neurodegeneration by reducing the rate of the autophagic clearance of misfolded proteins.[43] Interestingly, although lysosomes are mainly located near the nucleus of neurons under normal conditions, they were also observed in the axons of *lurcher* Purkinje cells,[39] suggesting that under some conditions, lysosomes may be formed at or transported to axons and may help the clearance of autophagosomes locally. Further studies are warranted to clarify the mechanisms by which the number and movement of autophagosomes and lysosomes are controlled in axons under physiological and pathological conditions.

Materials and Methods

Animals. *GFP-LC3* transgenic mice (B57BL/6J) were generated as described previously[17] and crossed with neural cell-specific *Atg5* deficient mice (*Atg5*$^{flox/flox}$; nestin-*Cre*, 129xB57BL/6J).[5] Genotyping for the *GFP-LC3*, *Atg5*^{flox} and the *Cre* gene has been described previously.[5,17] ICR mice were purchased from SLC (Hamamatsu, Japan). All procedures relating to the care and treatment of the animals were performed in accordance with the NIH guidelines. The animals were killed by decapitation after anesthetization with tribromoethanol.

Virus preparation and cerebellar infection. The expression plasmid of pPDGF-synaptophysin-EGFP were kindly provided by Dr. Y. Goda (University College London, London, UK). The cDNA encoding EGFP in the plasmid was replaced by that of DsRed-Monomer (DsRed) (Clontech, 632466) and subcloned into pCL20cMSCV vector[44] to produce pCL20cMSCV-synaptophysin-DsRed. Vesicular Stomatitis Virus-G protein (VSV-G) pseudotyped lentiviral vectors were provided by St. Jude Children's Research Hospital (Memphis, TN, USA). Virus particles were produced according to the method described earlier.[45] Briefly, human embryonic kidney (HEK) 293T cells were transfected with a mixture of four plasmids, pCAGkGP1R, pCAG4RTR2, pCAG-VSV-G and pCL20cMSCV-synaptophysin-DsRed, by a calcium phosphate precipitation method. Sixteen hours after transfection, the cells were washed with phosphate-buffered saline (PBS) twice and then cultured for an additional 24 h. The medium containing virus particles was harvested 40 h after transfection, filtered and centrifuged at 25,000 rpm for 90 min. The virus particles were finally suspended in PBS (pH 7.4), frozen in aliquots, and stored at -80°C. The titers of virus stocks were measured by transducing HEK 293T cells. Cerebellar microexplant cultures were infected with lentivirus at 7 d in vitro and incubated for additional 7 d for live-cell imaging.

Cell cultures. Cerebellar microexplant cultures were prepared as described previously.[46] Briefly, the cerebella from 5- to 7-day-old *GFP-LC3* or *GFP-LC3*; *Atg5*$^{flox/flox}$; nestin-*Cre* transgenic mice were isolated, freed from meninges and the choroid plexus using fine forceps, and cut into small pieces (30–50 μm) with scissors in ice-cold Hanks' balanced salt solution (Nacalai Tesque, 17460-15). The microexplants were washed three times, plated on 18-mm coverslips (Fisher Scientific) coated with poly-L-ornithine hydro bromide (Sigma, P4638), and maintained at

37°C with 5% CO_2 in a serum-free culture medium consisting of Neurobasal medium (Invitrogen, 21103-049) supplemented with 2.5 mM L-glutamine (Nacalai Tesque, 16919-55), 2.5% B-27 (Invitrogen, 0050129SA), and 0.01% penicillin/streptomycin. The cultured cells were used for experiments at 5–7 days in vitro.

Primary cultures of cerebellar granule cells were prepared from ICR mice on postnatal day 5–7, as described previously.[47] Cells were plated at a density of 2 x 10^5 cells on 35 mm-diameter dishes. Cells were maintained at 37°C with 5% CO_2 in a serum-free culture medium consisting of Neurobasal medium (Invitrogen, 21103-049) supplemented with 2.5 mM L-glutamine (Nacalai Tesque, 16919-55), 2.5% B-27 (Invitrogen, 0050129SA), and 0.01% penicillin/streptomycin. The cultured cells were used for experiments at 5–7 days in vitro.

Immunocytochemistry. Cultures were washed once in PBS and fixed with 4% paraformaldehyde for 20 min. After rinsing with PBS, the cells were permeabilized with 0.2% Triton X-100 in PBS with 2% normal goat serum and 2% bovine serum albumin for 1 h at 4°C. Immunocytochemical staining was performed using antibodies against microtubule-associated protein 2 (1:500; Millipore, AB5622), tau1 (1:100; Millipore, MAB3420) and lamp-1 (1:100; Stressgen, VAM-EN001), followed by incubation with Alexa 488- and Alexa 546-conjugated secondary antibodies (1:1,000; Molecular Probes). The stained cells were viewed using a fluorescence microscope (Nikon) or a confocal laser-scanning microscope (Fluoview; Olympus).

Live-cell imaging. For the time-lapse imaging experiments, the cover slips were transferred to an experimental chamber, washed three times, and resuspended in artificial cerebrospinal fluid solution (110 mM NaCl, 5 mM KCl, 1 mM $CaCl_2$, 10 mM glucose and 20 mM HEPES, pH 7.3 with KOH). Cells were maintained at 35°C by heating the experimental chamber (Medical systems corp, TC-202). The fluorescence of GFP-LC3 was visualized under an inverted microscope (Olympus, IX-70) and a 60x objective (NA 1.42; Olympus) using standard filter sets and a mercury lamp. Sequential images were acquired with a cooled CCD camera (Hamamatsu Photonics, ORCA-ER) equipped with a motorized filter wheel (Sutter Instrument, Lambda 10-2) controlled by the TI Work Bench software (written by T. Inoue). Images were taken every 10 s for 5 min. The distance each GFP-LC3 dot moved between two frames was measured using TI Work Bench. The mean number of autophagosomes was calculated by counting the number of GFP-LC3 dots in 30 randomly set 10-μm-long axon regions that were located farther than 200 μm from the microexplant core.

Western blot analysis. Cultured granule cells were solubilized in TNE buffer (50 mM NaF, 1% NP-40, 20 mM EDTA, 1 μM pepstatins, 2 μg/ml leupeptin, 10 μg/ml aprotinin, 0.1% SDS, 50 mM Tris-HCl, pH 8.0) for 1 h at 4°C. Soluble and insoluble fractions were separated by centrifugation at 11,500 x*g* for 20 min. Both fractions were incubated in SDS-PAGE sample buffer for 5 min at 95°C. After centrifugation, the supernatant was loaded onto SDS-polyacrylamide gels. The proteins were transferred to polyvinylidene difluoride membranes (Immobilon-P, Millipore), allowed to react with antibodies against LC3 (1:500) (Nanotool, 0231-100), p62/SQSTM1 (1:100) (Progen, GP62-C) or actin (1:500) (Sigma, A4700). Proteins were visualized using the chemiluminescence detection system ECL Plus (Amersham Pharmacia).

Chemicals. EHNA (erythro-9-[3-(2-hydroxynonyl)] adenine) (Sigma, E114), NMDA (*N*-methyl-D-aspartate) (Sigma, M3262), glycine (Sigma, 15527), APV (D-2-Amino-5-phosphono-valeric acid) (Sigma, A5282), and bafilomycin A1 (Wako, 023-11641) were used in this study.

Data analysis. The results are presented as the means ± SEM, and a p value < 0.05 was considered significant. The data were evaluated using an unpaired Student's t test. Nonparametric data were evaluated using the Mann-Whitney *U* test using Statview software (SAS Institute Inc.,).

Acknowledgements

We thank Sakae Narumi for technical assistance. This work was supported by a Grant-in-Aid from the Ministry of Education, Culture, Sports, Science and Technology of Japan (M.Y.), the Takeda Science Foundation (M.Y.), and the Japan Society for the Promotion of Science (J.N.).

Note

Supplementary materials can be found at:
www.landesbioscience.com/supplement/KatsumataAUTO6-3-Sup.pdf
www.landesbioscience.com/supplement/KatsumataAUTO6-3-Sup.mpeg

References

1. Reggiori F, Klionsky DJ. Autophagy in the eukaryotic cell. Eukaryot Cell 2002; 1:11-21.
2. Klionsky DJ, Cregg JM, Dunn WA Jr, Emr SD, Sakai Y, Sandoval IV, et al. A unified nomenclature for yeast autophagy-related genes. Dev Cell 2003; 5:539-45.
3. Kuma A, Hatano M, Matsui M, Yamamoto A, Nakaya H, Yoshimori T, et al. The role of autophagy during the early neonatal starvation period. Nature 2004; 432:1032-6.
4. Komatsu M, Waguri S, Ueno T, Iwata J, Murata S, Tanida I, et al. Impairment of starvation-induced and constitutive autophagy in Atg7-deficient mice. J Cell Biol 2005; 169:425-34.
5. Hara T, Nakamura K, Matsui M, Yamamoto A, Nakahara Y, Suzuki-Migishima R, et al. Suppression of basal autophagy in neural cells causes neurodegenerative disease in mice. Nature 2006; 441:885-9.
6. Komatsu M, Waguri S, Chiba T, Murata S, Iwata J, Tanida I, et al. Loss of autophagy in the central nervous system causes neurodegeneration in mice. Nature 2006; 441:880-4.
7. Komatsu M, Wang QJ, Holstein GR, Friedrich VL Jr, Iwata J, Kominami E, et al. Essential role for autophagy protein Atg7 in the maintenance of axonal homeostasis and the prevention of axonal degeneration. Proc Natl Acad Sci USA 2007; 104:14489-94.
8. Nishiyama J, Miura E, Mizushima N, Watanabe M, Yuzaki M. Aberrant membranes and double-membrane structures accumulate in the axons of Atg5-null Purkinje cells before neuronal death. Autophagy 2007; 3:591-6.
9. Kroemer G, Levine B. Autophagic cell death: the story of a misnomer. Nat Rev Mol Cell Biol 2008; 9:1004-10.
10. Cuervo AM. Autophagy: in sickness and in health. Trends Cell Biol 2004; 14:70-7.
11. Rubinsztein DC, DiFiglia M, Heintz N, Nixon RA, Qin ZH, Ravikumar B, et al. Autophagy and its possible roles in nervous system diseases, damage and repair. Autophagy 2005; 1:11-22.
12. Boland B, Kumar A, Lee S, Platt FM, Wegiel J, Yu WH, et al. Autophagy induction and autophagosome clearance in neurons: relationship to autophagic pathology in Alzheimer's disease. J Neurosci 2008; 28:6926-37.
13. Ravikumar B, Vacher C, Berger Z, Davies JE, Luo S, Oroz LG, et al. Inhibition of mTOR induces autophagy and reduces toxicity of polyglutamine expansions in fly and mouse models of Huntington disease. Nat Genet 2004; 36:585-95.
14. Cai ZL, Shi JJ, Yang YP, Cao BY, Wang F, Huang JZ, et al. MPP+ impairs autophagic clearance of alpha-synuclein by impairing the activity of dynein. Neuroreport 2009; 20:569-73.

15. Borsello T, Croquelois K, Hornung JP, Clarke PG. N-methyl-d-aspartate-triggered neuronal death in organotypic hippocampal cultures is endocytic, autophagic and mediated by the c-Jun N-terminal kinase pathway. Eur J Neurosci 2003; 18:473-85.
16. Tarabal O, Caldero J, Casas C, Oppenheim RW, Esquerda JE. Protein retention in the endoplasmic reticulum, blockade of programmed cell death and autophagy selectively occur in spinal cord motoneurons after glutamate receptor-mediated injury. Mol Cell Neurosci 2005; 29:283-98.
17. Mizushima N, Yamamoto A, Matsui M, Yoshimori T, Ohsumi Y. In vivo analysis of autophagy in response to nutrient starvation using transgenic mice expressing a fluorescent autophagosome marker. Mol Biol Cell 2004; 15:1101-11.
18. Yang Y, Fukui K, Koike T, Zheng X. Induction of autophagy in neurite degeneration of mouse superior cervical ganglion neurons. Eur J Neurosci 2007; 26:2979-88.
19. Yue Z. Regulation of neuronal autophagy in axon: implication of autophagy in axonal function and dysfunction/degeneration. Autophagy 2007; 3:139-41.
20. Kuma A, Matsui M, Mizushima N. LC3, an autophagosome marker, can be incorporated into protein aggregates independent of autophagy: caution in the interpretation of LC3 localization. Autophagy 2007; 3:323-8.
21. Yamasaki T, Kawaji K, Ono K, Bito H, Hirano T, Osumi N, et al. Pax6 regulates granule cell polarization during parallel fiber formation in the developing cerebellum. Development 2001; 128:3133-44.
22. Nakatsuji N, Nagata I. Paradoxical perpendicular contact guidance displayed by mouse cerebellar granule cell neurons in vitro. Development 1989; 106:441-7.
23. Kawaji K, Umeshima H, Eiraku M, Hirano T, Kengaku M. Dual phases of migration of cerebellar granule cells guided by axonal and dendritic leading processes. Mol Cell Neurosci 2004; 25:228-40.
24. Ekstrom P, Kanje M. Inhibition of fast axonal transport by erythro-9-[3-(2-hydroxynonyl)]adenine. J Neurochem 1984; 43:1342-5.
25. Forman DS, Brown KJ, Promersberger ME. Selective inhibition of retrograde axonal transport by erythro-9-[3-(2-hydroxynonyl)]adenine. Brain Res 1983; 272:194-7.
26. Koike M, Shibata M, Waguri S, Yoshimura K, Tanida I, Kominami E, et al. Participation of autophagy in storage of lysosomes in neurons from mouse models of neuronal ceroid-lipofuscinoses (Batten disease). Am J Pathol 2005; 167:1713-28.
27. Klionsky DJ, Abeliovich H, Agostinis P, Agrawal DK, Aliev G, Askew DS, et al. Guidelines for the use and interpretation of assays for monitoring autophagy in higher eukaryotes. Autophagy 2008; 4:151-75.
28. Yamamoto A, Tagawa Y, Yoshimori T, Moriyama Y, Masaki R, Tashiro Y. Bafilomycin A1 prevents maturation of autophagic vacuoles by inhibiting fusion between autophagosomes and lysosomes in rat hepatoma cell line, H-4-II-E cells. Cell Struct Funct 1998; 23:33-42.
29. Mizushima N, Yoshimori T. How to interpret LC3 immunoblotting. Autophagy 2007; 3:542-5.
30. Rubinsztein DC, Cuervo AM, Ravikumar B, Sarkar S, Korolchuk V, Kaushik S, et al. In search of an "autophagomometer". Autophagy 2009; 5:585-9.
31. Bjorkoy G, Lamark T, Brech A, Outzen H, Perander M, Overvatn A, et al. p62/SQSTM1 forms protein aggregates degraded by autophagy and has a protective effect on huntingtin-induced cell death. J Cell Biol 2005; 171:603-14.
32. Yue Z, Holstein GR, Chait BT, Wang QJ. Using genetic mouse models to study the biology and pathology of autophagy in the central nervous system. Methods Enzymol 2009; 453:159-80.
33. Selimi F, Lohof AM, Heitz S, Lalouette A, Jarvis CI, Bailly Y, et al. Lurcher GRID2-induced death and depolarization can be dissociated in cerebellar Purkinje cells. Neuron 2003; 37:813-9.
34. Kimura S, Noda T, Yoshimori T. Dynein-dependent movement of autophagosomes mediates efficient encounters with lysosomes. Cell Struct Funct 2008; 33:109-22.
35. Jahreiss L, Menzies FM, Rubinsztein DC. The itinerary of autophagosomes: from peripheral formation to kiss-and-run fusion with lysosomes. Traffic 2008; 9:574-87.
36. Shacka JJ, Lu J, Xie ZL, Uchiyama Y, Roth KA, Zhang J. Kainic acid induces early and transient autophagic stress in mouse hippocampus. Neurosci Lett 2007; 414:57-60.
37. Zuo J, De Jager PL, Takahashi KA, Jiang W, Linden DJ, Heintz N. Neurodegeneration in Lurcher mice caused by mutation in delta2 glutamate receptor gene. Nature 1997; 388:769-73.
38. Kohda K, Wang Y, Yuzaki M. Mutation of a glutamate receptor motif reveals its role in gating and delta2 receptor channel properties. Nat Neurosci 2000; 3:315-22.
39. Wang QJ, Ding Y, Kohtz DS, Mizushima N, Cristea IM, Rout MP, et al. Induction of autophagy in axonal dystrophy and degeneration. J Neurosci 2006; 26:8057-68.
40. Nishiyama J, Matsuda K, Kakegawa W, Yamada N, Motohashi J, Mizushima N, et al. Reevaluation of neurodegeneration in lurcher mice: constitutive ion fluxes cause cell death with, not by, autophagy. J Neurosci in press.
41. Lakadamyali M, Rust MJ, Babcock HP, Zhuang X. Visualizing infection of individual influenza viruses. Proc Natl Acad Sci USA 2003; 100:9280-5.
42. Bannai H, Inoue T, Nakayama T, Hattori M, Mikoshiba K. Kinesin dependent, rapid, bi-directional transport of ER sub-compartment in dendrites of hippocampal neurons. J Cell Sci 2004; 117:163-75.
43. Ravikumar B, Acevedo-Arozena A, Imarisio S, Berger Z, Vacher C, O'Kane CJ, et al. Dynein mutations impair autophagic clearance of aggregate-prone proteins. Nat Genet 2005; 37:771-6.
44. Hanawa H, Kelly PF, Nathwani AC, Persons DA, Vandergriff JA, Hargrove P, et al. Comparison of various envelope proteins for their ability to pseudotype lentiviral vectors and transduce primitive hematopoietic cells from human blood. Mol Ther 2002; 5:242-51.
45. Torashima T, Okoyama S, Nishizaki T, Hirai H. In vivo transduction of murine cerebellar Purkinje cells by HIV-derived lentiviral vectors. Brain Res 2006; 1082:11-22.
46. Forrest D, Yuzaki M, Soares HD, Ng L, Luk DC, Sheng M, et al. Targeted disruption of NMDA receptor 1 gene abolishes NMDA response and results in neonatal death. Neuron 1994; 13:325-38.
47. Kurschner C, Yuzaki M. Neuronal interleukin-16 (NIL-16): a dual function PDZ domain protein. J Neurosci 1999; 19:7770-80.

Regional Spinal Cord Cooling Using a Countercurrent Closed-Lumen Epidural Catheter

Hideyuki Shimizu, MD, PhD, Atsuo Mori, MD, PhD, Tatsuya Yamada, MD, PhD, Akiko Ishikawa, MD, Hideyuki Okano, MD, PhD, Junzo Takeda, MD, PhD, and Ryohei Yozu, MD, PhD

Departments of Cardiovascular Surgery, Anesthesiology, and Physiology, Keio University, Shinjuku-ku, Tokyo, Japan

We developed a method of regional spinal cord cooling by using an epidural catheter containing cold saline in its isolated counter-current lumen. We describe the clinical application of this innovative procedure to the prevention of paraplegia during surgery for thoracic and thoracoabdominal aortic aneurysms.

(Ann Thorac Surg 2010;89:1312–3)

Paraplegia associated with surgery for thoracic and thoracoabdominal aortic aneurysm remains a devastating complication. We previously demonstrated the ability of regional spinal cord cooling using a custom-designed epidural catheter to prevent ischemic spinal cord injury in experimental studies using pigs [1, 2]. We applied this novel system in a clinical setting.

HEATURE ARTICLES

Technique

Patients

Six patients (4 men, 2 women; aged 57 to 80 years) with aneurysms of the descending thoracic (5 patients) or thoracoabdominal (1 patient) aorta underwent elective surgery using our novel cooling method between September 2008 and January 2009. The cause of aortic disease was atherosclerotic aneurysm (n = 3), aortic dissection (n = 2), and pseudoaneurysm after infection (n = 1). Four of the 6 patients had prior operations on the abdominal aorta (n = 2), the transverse aorta (n = 1), and both (n = 1). The Institutional Review Board of Keio University Hospital approved the study, and written, informed consent was obtained from each patient to participate in all procedures associated with the study.

Continuous Cord Cooling System Using a Custom-Designed Epidural Catheter

A custom-designed polyurethane epidural catheter (Unitika, Tokyo, Japan) (Fig 1), an external circuit tube, and a pump with a hollow fiber heat exchanger (Senko-Ika Co, Ltd, Tokyo, Japan) comprised a circuit (Fig 2). The catheter (16-gauge outer diameter; length, 30 cm) has two ends that form the inlet and outlet of a single U-shaped closed lumen inside it. The direction of the flow of saline infused from the inlet reverses at the tip of the catheter and flows out of the outlet. The temperature of the saline is reduced to 12°C to 13°C by a cooling unit, infused into the inlet of the countercurrent catheter and then circulated by an external roller pump at an approximate flow rate of 60 mL/min.

Percutaneous Installation of Cooling Catheter

The catheter was positioned percutaneously on the day before surgery. Patients were placed in the prone position. A local anesthetic was applied and then the skin on the back was punctured with a special epidural Touhy-type needle with a thin polyurethane outer-sheath (Unisis-Unitika, Tokyo, Japan) through the paramedian approach at level 1 to 2 of the lumbar spine. The needle was advanced until the tip reached the epidural space and then removed without moving the outer sheath. The cooling catheter was introduced into the epidural space through the outer sheath, and was advanced in the direction of the head as far as it could contact the segment of the spinal cord that would be under ischemic stress during aortic cross clamping. Fluoroscopic guidance confirmed the proper placement, after which the outer sheath was peeled off. The catheter was affixed to the skin and left in situ until surgery.

Surgical Procedure, External Corporeal Bypass, and Epidural Cooling Protocol

Surgery proceeded with patients in the right-sided lateral position. A left thoracotomy was performed through an appropriate intercostal space. The skin incision was extended toward the umbilicus, and the diaphragm was divided in 1 patient with a thoracoabdominal aortic aneurysm. Heparin sulfate was injected intravenously, and then a femoro-femoral bypass with a centrifugal pump and a membrane oxygenator was established for distal perfusion during aortic cross clamping. We did not actively cool the blood with an external heat-exchanger, although the rectal temperature spontaneously dropped to 33.6°C to 36.2°C. The aorta was cross clamped using the serial shift technique in 2 patients and was replaced with prosthetic grafts. The intercostal arteries were reconstructed in a beveled fashion in 4 patients, and the celiac and superior mesenteric arteries were reconstructed using a branched graft in 1. Regional spinal cord cooling was started 30 minutes beforehand, continued during aortic cross clamping, and terminated 30 minutes after unclamping. None of the patients underwent cerebrospinal fluid drainage. Motor-evoked potentials (MEPs) were monitored in all patients.

Accepted for publication June 9, 2009.

Address correspondence to Dr Shimizu, Department of Cardiovascular Surgery, 35 Shinanomachi, Shinjuku-ku, Tokyo, 160-8582, Japan; e-mail: hideyuki@sc.itc.keio.ac.jp.

Published by Elsevier Inc

0003-4975/10/$36.00
doi:10.1016/j.athoracsur.2009.06.045

Results

The mean durations of aortic cross clamping and external corporeal bypass were 52.0 ± 18.7 and 65.3 ± 19.5 minutes, respectively. Motor-evoked potentials did not disappear during or after aortic cross clamping in any of the patients, and none of them died in the hospital. All patients recovered full use of their lower limbs with no paraplegia or paraparesis on the day of surgery. Complications, including coagulopathy and cardiac events, did not arise.

Comment

Paraplegia remains the most serious complication associated with thoracic and thoracoabdominal aortic aneurysm. Hypothermia is one of the most reliable methods of protecting the spinal cord from ischemia, but systemic hypothermia confers several risks, including coagulopathy, arrhythmia, and lung dysfunction. Cambria and coworkers [3] described favorable clinical results of local cooling by infusing iced saline into the epidural space during aortic cross clamping. However, it might cause a detrimental increase in cerebrospinal fluid pressure. To avoid such adverse effects, we developed an alternative technique for epidural cooling using a custom-designed countercurrent catheter. We demonstrated in pigs that a cooling catheter containing saline at a temperature of 4°C circulating at a flow rate of 45 mL/min could cool the spinal cord by 9.7°C without elevating cerebrospinal fluid pressure. The spinal cord was protected from 45 minutes of ischemia, induced by aortic cross clamping without distal perfusion [1, 2]. Based on these results as well as the outlet temperature of the circulating saline, we determined the cooling conditions for clinical applications.

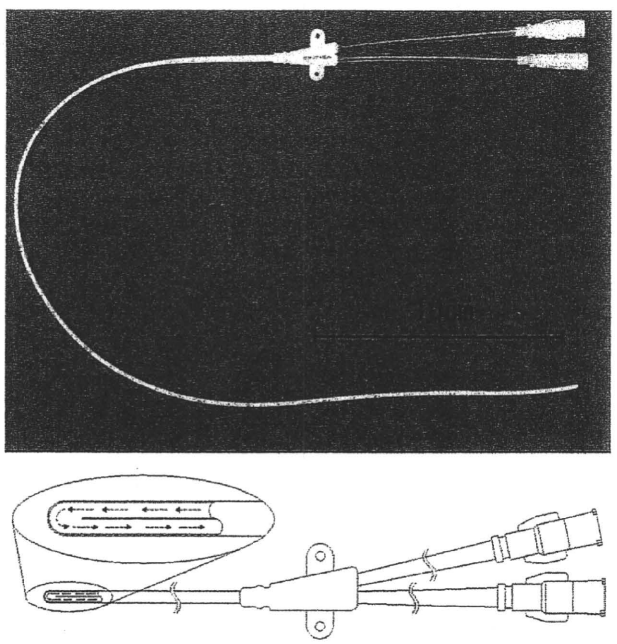

Fig 1. Epidural cooling catheter. Cold saline circulates in closed lumen of catheter, turning back at tip without leakage.

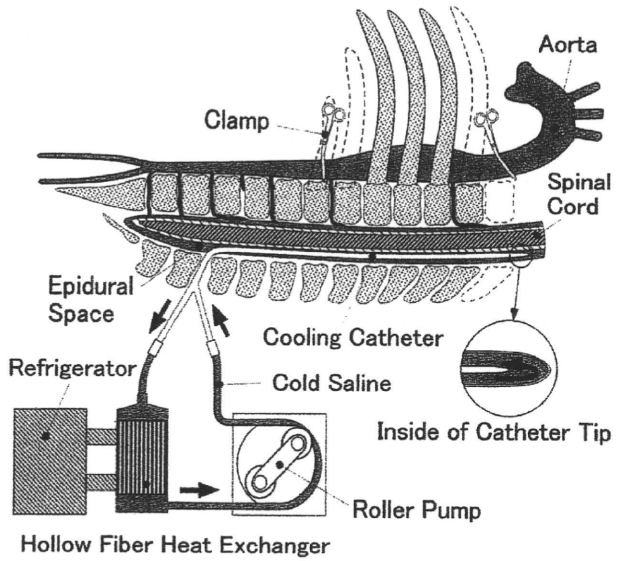

Fig 2. Schematic illustration of continuous cord cooling system. Closed loop circuit comprises epidural cooling catheter, circulating pump, and hollow-fiber cooling unit.

We did not measure cerebrospinal fluid temperature and pressure to avoid the complexity of installing another catheter. However, such measurements might be helpful to rigorously adjust cooling conditions for each individual. The combination of epidural cooling and cerebrospinal fluid drainage might be a promising strategy.

We also developed a Touhy-style epidural needle with an outer sheath that can be peeled off. This modification allowed installation of the catheter into the epidural space without laminectomy, similar to epidural pacing lead placement against phantom pain control.

Although our patient cohort was small, the clinical application of regional spinal cord cooling using a custom-designed countercurrent epidural catheter proved successful as an additional protection against paraplegia. Further clinical trials are warranted to confirm that this technique protects against paraplegia during surgery for thoracic and thoracoabdominal aortic aneurysms.

This study was supported by a Grant-in-Aid for Scientific Research (C) of the Ministry of Education, Culture, Sports, Science, and Technology. We express special thanks to Nobuyuki Kabei, PhD for excellent technical assistance.

References

1. Mori A, Ueda T, Hachiya T, et al. An epidural cooling catheter protects the spinal cord against ischemic injury in pigs. Ann Thorac Surg 2005;80:1829–34.
2. Yoshitake A, Mori A, Shimizu H, et al. Use of an epidural cooling catheter with a closed countercurrent lumen to protect against ischemic spinal cord injury in pigs. J Thorac Cardiovasc Surg 2007;134:1220–6.
3. Cambria RP, Clouse WD, Davison JK, Dunn PF, Corey M, Dorer D. Thoracoabdominal aneurysm repair: results with 317 operations performed over a 15-year interval. Ann Surg 2002;236:471–9.